



Review

# Advancements in Metal Additive Manufacturing: A Comprehensive Review of Material Extrusion with Highly Filled Polymers

Mahrukh Sadaf <sup>1,2,\*</sup>, Mario Bragaglia <sup>2</sup>, Lidija Slemenik Perše <sup>1</sup> and Francesca Nanni <sup>2</sup>

<sup>1</sup> Laboratory of Experimental Mechanics, Faculty for Mechanical Engineering, University of Ljubljana, Aškerčeva Ulica 6, 1000 Ljubljana, Slovenia; lidija.slemenik.perse@fs.uni-lj.si

<sup>2</sup> Department of Enterprise Engineering “Mario Lucertini”, INSTM RU Roma-Tor Vergata, University of Rome “Tor Vergata”, Via del Politecnico 1, 00133 Rome, Italy; bragaglia@ing.uniroma2.it (M.B.); fnanni@ing.uniroma2.it (F.N.)

\* Correspondence: mahrukh.sadaf@fs.uni-lj.si; Tel.: +386-1-6207-107

**Abstract:** Additive manufacturing (AM) has attracted huge attention for manufacturing metals, ceramics, highly filled composites, or virgin polymers. Of all the AM methods, material extrusion (MEX) stands out as one of the most widely employed AM methods on a global scale, specifically when dealing with thermoplastic polymers and composites, as this technique requires a very low initial investment and usage simplicity. This review extensively addresses the latest advancements in the field of MEX of feedstock made of polymers highly filled with metal particles. After developing a 3D model, the polymeric binder is removed from the 3D-printed component in a process called debinding. Furthermore, sintering is conducted at a temperature below the melting temperature of the metallic powder to obtain the fully densified solid component. The stages of MEX-based processing, which comprise the choice of powder, development of binder system, compounding, 3D printing, and post-treatment, i.e., debinding and sintering, are discussed. It is shown that both 3D printing and post-processing parameters are interconnected and interdependent factors, concurring in determining the resulting mechanical properties of the sintered metal. In particular, the polymeric binder, along with its removal, results to be one of the most critical factors in the success of the entire process. The mechanical properties of sintered components produced through MEX are generally inferior, compared with traditional techniques, as final MEX products are more porous.

**Keywords:** additive manufacturing; debinding; feedstock; material extrusion; metal injection molding; metals; sintering



**Citation:** Sadaf, M.; Bragaglia, M.; Slemenik Perše, L.; Nanni, F. Advancements in Metal Additive Manufacturing: A Comprehensive Review of Material Extrusion with Highly Filled Polymers. *J. Manuf. Mater. Process.* **2024**, *8*, 14. <https://doi.org/10.3390/jmmp8010014>

Academic Editors: Mohammad J. Mirzaali and Steven Y. Liang

Received: 10 November 2023

Revised: 10 January 2024

Accepted: 13 January 2024

Published: 16 January 2024



**Copyright:** © 2024 by the authors. Licensee MDPI, Basel, Switzerland. This article is an open access article distributed under the terms and conditions of the Creative Commons Attribution (CC BY) license (<https://creativecommons.org/licenses/by/4.0/>).

## 1. Introduction

Among the widely adopted techniques in the global landscape of additive manufacturing (AM), material extrusion (MEX), also termed fused filament fabrication, stands out, particularly for applications involving thermoplastic composites and polymers due to the advantages of low initial investment, short processing time, minimal material wastage, user-friendly operation, precise control of processing parameters, the capacity for simultaneous use of multiple materials (multi-material 3D printing), and seamless integration with diverse computer-aided design (CAD) software [1–8]. Additionally, MEX offers the advantage of directly fabricating finished products, eliminating the need for molds, dies, or tooling, which are notable constraints in conventional manufacturing processes [9–12].

MEX has garnered widespread application across diverse industries. Notably, in aerospace, it contributes to the production of intricately designed components that are both lightweight and exceptionally durable, thereby optimizing fuel efficiency and overall performance. Within the medical sector, MEX enables the fabrication of tailor-made implants and anatomical models, redefining preoperative planning and advancing surgical training

processes. Additionally, in the realm of consumer goods, this technology empowers designers to craft highly customizable products characterized by intricate geometries, ushering in a new era of personalized and sophisticated manufacturing solutions [13–17]. Figure 1 illustrates a schematic representation of extrusion-based AM, categorized into three types based on the type of extruder head employed.

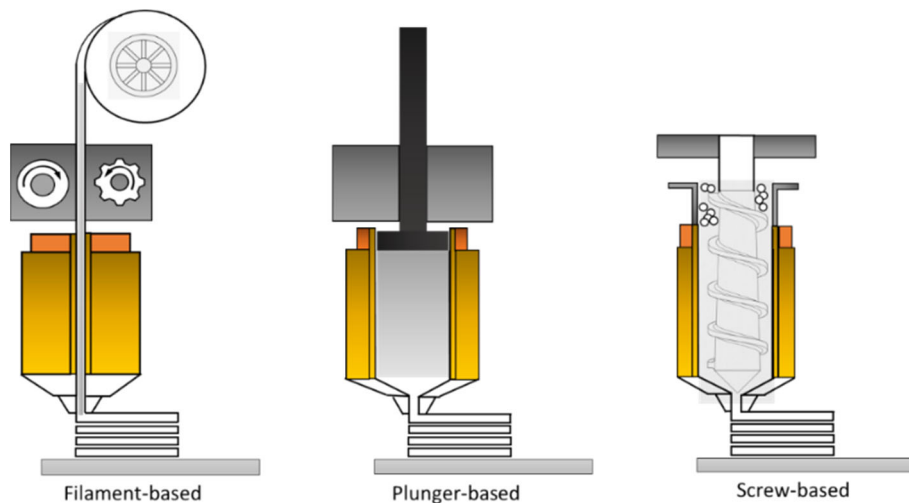


**Figure 1.** Diverse categorizations and approaches in extrusion-based AM (adapted from [14]).

### 1.1. Material Extrusion with Filaments

MEX with filaments, also referred to as fused filament fabrication (FFF), stands out as the predominant method within the broader material extrusion process. This technique was pioneered in the late 1980s by S. Scott Crump and subsequently gained commercial traction, with Stratasys trademarking it as Fused Deposition Modeling (FDM) specifically for thermoplastic polymers like PLA or ABS [4,18,19].

In MEX, the process involves working with polymer-based filaments or filaments comprising polymer matrix composites. The procedure commences with a spooled filament (diameter of 1.75 mm or 3 mm), being fed to the printing apparatus through a mechanism involving two counter-rotating rollers. These rollers are equipped with teeth or grooves, which ensure a secure grip on the filament, preventing any slippage issues [3]. Subsequently, the filament moves into the liquefier segment, where it undergoes melting. Fundamentally, the unmelted filament (often composed of polymer or composite-based polymer), acts as a piston, propelling the melted portion and facilitating its passage through the orifice or nozzle. To achieve this, the material is heated to a temperature slightly above its melting point, with the specific temperature being determined by the type of material being utilized [20].

Tailoring the printing bed temperature to suit the characteristics of each material is a common practice aimed at enhancing layer adhesion [3,21]. MEX printing typically operates along three axes ( $x$ ,  $y$ ,  $z$ ), with the printer orchestrating parameters such as flow rate, the position of the liquefier along the  $x$ - $y$ -axes, and the  $z$ -axis position. Subsequently, the material is extruded through the orifice and deposited as a molten strand within the component [4]. Most commercial MEX machines are furnished with only one extrusion head. However, within the MEX framework, there exists the flexibility to incorporate two or more extrusion heads. This feature permits the simultaneous use of diverse materials or colors in the same object or layer, enabling multi-material fabrication [3,19,22].

It is important to note that this filament-based technique does have some constraints concerning the range of materials it can accommodate. The filament must possess the right balance of flexibility for spooling, strength to prevent buckling, and a consistent diameter to ensure uninterrupted mass flow (preventing from over- or under-extrusion). To address

some of these challenges, two novel feeding systems have been established: screw extrusion and plunger/syringe-based MEX [14,23].

### 1.2. Material Extrusion with Plungers

At present, two American companies, namely, Markforged Inc. (Waltham, MA, USA) and Desktop Metal Inc. (Burlington, MA, USA) [24], have introduced machines based on syringe-fed material extrusion (MEX). Markforged labels their approach as atomic diffusion additive manufacturing (ADAM), while Desktop Metal refers to theirs as bound metal deposition. This method involves employing specially shaped rods composed of a thermoplastic binder system combined with ceramic or metallic powder for reinforcement. The fundamental process involves inserting these feeding rods into cartridges, which are subsequently introduced into the heating unit. Within this unit, the material undergoes a softening process, rendering it suitable for extrusion.

The molten material gathers within a reservoir, and a mechanical pushing mechanism propels the softened material, depositing it onto the printing bed in a meticulously layered manner, following the path delineated by the generated 3D model [14,24,25]. It can be noted that the operational principle of syringe-based MEX machines closely resembles the technologies employed in robocasting. In this context, the construction material (rods) incorporates a thermoplastic-based binder, as opposed to the utilization of water as a binder in robocasting [26,27]. This methodology typically finds applications in the biomedical field, where the necessity of biocompatibility is vital [28]. Bose et al. [29] magnificently processed dense tungsten alloy using syringe-based MEX equipment, achieving commendable densification exceeding 98% of the theoretical density.

### 1.3. Material Extrusion with Screws

Screw-driven material extrusion presents a distinct advantage by directly utilizing pellets within the barrel, avoiding the additional step of producing filaments or rods. This technique finds widespread use in the plastics processing sector for fabricating uniform, intricately shaped components. A screw extruder is partitioned into distinct zones, initiating with the feeding section, where pellets are conveyed to the melting zone; pellets then undergo softening via friction and heat before progressing to the metering zone. Subsequently, the molten material encounters high pressure before being expelled through the orifice or nozzle [14,23,30]. Maintaining control over pellet size is pivotal to ensuring the ultimate product's quality and achieving a consistent flow of extruded material [31].

Numerous enterprises, such as AIM3D GmbH (Rostock, Germany) [32,33] and Pollen AM Inc. (Paris, France) [34,35] are actively commercializing screw-based MEX machines. Furthermore, Oak Ridge National Laboratories (Oak Ridge, TN, USA) and Cincinnati Inc. (Cincinnati, OH, USA) have engineered a screw extrusion machine tailored for large-scale production. This system, termed “big area additive manufacturing” or BAAM, has been developed [36,37]. The recent literature showcases several successful endeavors involving screw-based MEX equipment utilized with highly filled composite materials, including 17-4PH steel [38–41], tool steel [42], and 316L stainless steel [1,43–45].

## 2. Fabrication of Metal Objects with High-Loaded Powders Using Filament-Based Material Extrusion (MEX)

The feedstock used for MEX is like the one employed in a widely utilized manufacturing process known as metal injection molding (MIM). In MIM, the feedstock is extruded and subsequently injected into a mold cavity to shape the desired green form. In MEX, after the feedstock is prepared, the next step involves crafting a filament loaded with a substantial amount of metallic powder. This filament is then subjected to 3D printing using a standard MEX printer. The ultimate post-processing steps remain consistent across both manufacturing methods (i.e., debinding and sintering). The stages of MEX-based processing comprise choice of powder, development of binder system, compounding, shaping, debinding, and sintering. An illustrative overview of these stages is presented in Figure 2.

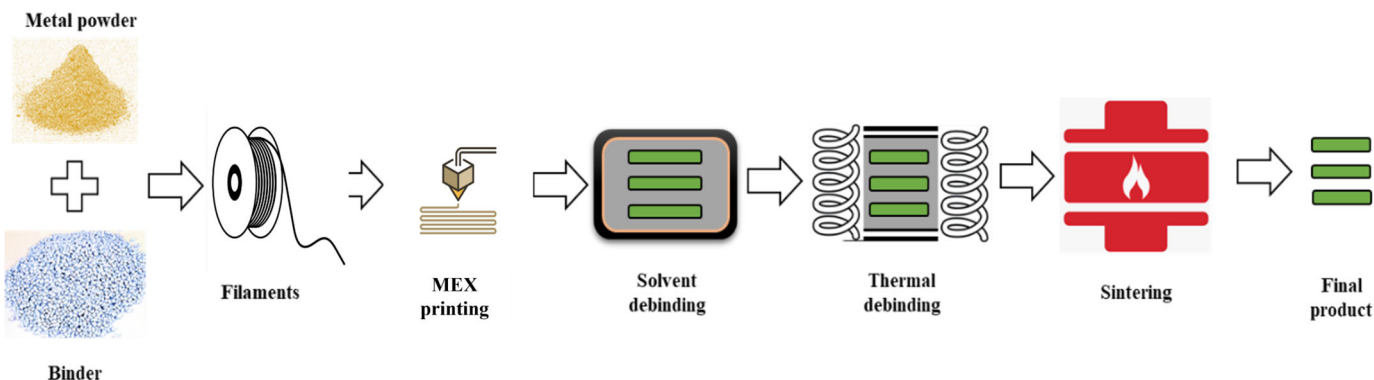


**Figure 2.** Schematic overview for material extrusion based on highly loaded metallic powder with the examples of standard bending bars [46].

### 2.1. Choice of Powder

The mechanical properties of the end components are associated with the metallic powder fraction within the feedstock. The final MEX component exhibits the same properties as the starting powder's metal. For a metallic powder to be suitable for fabricating MEX components, it must satisfy the subsequent conditions [47,48]:

- The powder size has to be small;
- The powder has to disperse well with the binder;
- Sintering is required to have significant densification;
- The melting and sintering temperatures should be adequately elevated to avoid interfering with the debinding process.

The powder size, existing as a range of sizes rather than a single one, represents a constraining factor in MEX processing. Even though there is no lower size limit, the size of particles needs to be sufficiently small to avoid the blockage of the 3D printer nozzle/orifice (with a diameter scale of 0.2–0.8 mm) of the MEX equipment [14,29,49–52]. The powder employed in MEX fundamentally resembles the powder used in MIM. Mainly, metal injection molding (MIM) uses particle sizes with an average of 5 to 15  $\mu\text{m}$  [50]. Overall, in MEX, powders with  $D90 < 22 \mu\text{m}$  are usually chosen. In the work [53], Kukla et al. examined the influence of particle size on the physical characterization of highly filled 316 L stainless steel feedstocks for MEX. They established that the feedstock made of larger particles ( $D50 \approx 8.6 \mu\text{m}$ ) had lower stiffness, flexibility, and viscosity than the feedstock based on smaller particle size ( $D50 \approx 5.5 \mu\text{m}$ ). Following that, they also reported that coarse particle sizes lead to buckling while shaping, creating printability failures [54,55]. Thus, the selection of appropriate particle sizes is vital while working with MEX.

Apart from the particle size, an additional crucial aspect to consider is the morphology of the powder particles. The utilization of powders with a spherical shape leads to better flow properties and enhanced packing density compared with irregularly shaped particles [47]. Enhanced flowability is likely to lower the viscosity of the feedstock material by reducing resistance to movement within the binder matrix, ensuring printability even at high powder loadings [56,57]. Concurrently, the higher packing density allows a larger volume of powder to be included in the feedstock, leading to decreased overall shrinkage during the sintering process [56]. However, irregularly shaped powders can also be applicable for MEX printing. Irregular powders offer the benefits of being more cost-effective compared with spherical powders produced through gas atomization and better shape retention [56].

Numerous recent studies focusing on the debinding and sintering processes for achieving metallic components through MEX are available. The variety of powder types is detailed in Table 1.

**Table 1.** Metals investigated for utilization in MEX.

Metal	Powder Loading in Feedstock (vol.%)	Ref.
Stainless steel (316L)	50, 55 and 65	[14,38,43,46,58–63]
Stainless steel (17-4PH)	55, 60, and 64	[14,64–68]
Stainless steel (AISI 630)	79	[69]
Copper	≥55	[17,46,62,70–79]
Titanium (Ti-6Al-4V)	55 and 59	[56,80–84]
Carbonyl iron	65	[85]
Rare-earth magnets (NdFeB)	55	[86]
Tungsten carbide–cobalt	50	[66,67]

To achieve dense sintered metals, it is common to use high filler loading, typically ranging from 55% to 65% by volume. This range of metallic particles is essential to facilitating the sintering process, which involves diffusion mechanisms at the surface, lattice, and grain boundaries [87]. However, exceeding the recommended metallic loading (55–65% by volume) in the feedstock can reduce the printability of extruded filaments. Elevated metallic loading leads to increased viscosity and decreased stiffness [50]. When the filament lacks sufficient rigidity, there is a potential for complications in the automatic feeding process within the printing unit due to premature and brittle filament fractures while passing through the feeding gears. In a study by Gutierrez et al. [88], various types of metallic powders were investigated, revealing that the maximum printable filament volume content is largely dependent on the material. This dependency arises from the critical role of the particle–matrix chemical interface in determining mechanical properties.

## 2.2. Choice of Binder System

The second component of the feedstock is the binder system. This system primarily comprises three key constituents derived from diverse polymers, additives, and waxes [8,14,48,50,89–92]:

- Primary or main binder: This constituent holds the largest proportion within the formulation (it typically contains 50–90 vol.% of the whole binder system) and can be effectively removed at low temperatures. Commonly employed primary binder materials encompass carnauba wax; paraffin wax; sometimes agarose, in certain practices; etc. Waxes primarily serve to lower the feedstock's viscosity, achieving favorable flow characteristics, and to improve filament rigidity. However, waxes should be utilized within prescribed limits, as exceeding these limits can diminish the mechanical attributes of both filaments and the resulting printed object.
- Secondary or backbone binder: This element maintains the structural integrity of the product after the initial removal of the main binder during the first debinding phase. The secondary binder is typically eliminated through thermal degradation in the second stage of debinding, which then progresses to the sintering process. The proportion of the secondary binder ranges from 0% to 50% of the total binder system volume. Commonly utilized secondary binder materials include polypropylene (PP), low-density polyethylene (LDPE), high-density polyethylene (HDPE), ethylene vinyl acetate (EVA), polyethylene glycol (PEG), polystyrene (PS), and several others. These polymers have a short molecular chain length that permits them to decompose with relatively small volume variations, reducing the chance of problems during debinding and sintering. Other advantages of using these polymers are their highly availability, low cost, and less carbon contamination during burnout in the thermal debinding stage [48].
- Additives: Additional components, such as compatibilizers, stabilizers, dispersing agents, and surfactants, play a vital role in promoting effective diffusion between the powder and binder. These additives prevent phase separation and agglomeration. Additives typically constitute 0–10% of the total volume within the binder system. Among the commonly employed additives, stearic acid stands out as a frequently

used example. Furthermore, it is important to use additives within specified limits; surpassing these limits can lead to the formation of defects, such as bubbles and cracks, in the final product.

Examples of binder system constituents for MEX-based metal AM used in the literature are reported in Table 2.

**Table 2.** Examples of binder system constituents employed in MEX-based metal AM.

Backbone (10–50 vol.%)	Main Component (50–90 vol.%)	Additives (1–10 vol.%)	Ref.
Grafted high-density polyethylene (AA-HDPE)	Paraffin wax, styrene–ethylene–butylene copolymer (SEBS)	Stearic acid	[93]
Low-density polyethylene (LDPE)	Paraffin wax	Stearic acid	[73]
Low-density polyethylene (LDPE)	Paraffin wax	None	[31]
Polypropylene (PP)	Thermoplastic elastomer (TPE)	None	[94]
Ethylene vinyl acetate (EVA)	None	Stearic acid	[95]
Polyamide (PA)	Not disclosed	None	[2]
Thermoplastic elastomer (TPE)	Grafted polyolefin	Non-disclosed compatibilizer	[53,86,96–98]
Polyoxymethylene (POM)	Paraffin wax	None	[43]
Polymer LDPE	Elastomer and wax	Plasticizer	[59]
Polypropylene (PP)	LDPE wax	None	[1]
Poly (ethylene–vinyl acetate) copolymer	Elastomer	Wax	[99]
Not disclosed	Poly (propylene–ethylene) copolymer, poly (isobutene)	Stearic acid	[100]
	Polyolefin	Not disclosed	[83]

### 2.3. Compounding of Feedstock and Filaments

Once the suitable powder and binder components have been selected, the following stage is the compounding of feedstock. The process of preparing feedstock for MEX is like that of metal injection molding (MIM) feedstocks. This involves the thorough mixing of metal powder with a melted binder system. It is crucial to have good homogeneity between metallic powder and binder; otherwise, there is a risk of encountering issues such as irregular shrinkage and other potential defects [48].

In the compounding process [50], there are two types of equipment that can be utilized to manufacture the feedstock. The first type is a batch mixer, often employed for smaller production runs, and it is referred to as a kneader or a roller mixer, as illustrated in Figure 3. A conventional kneader comprises an internal mixer fitted with two counter-rotating rollers designed to operate at varying speeds. This arrangement generates high shear forces between the rotating rollers and the walls of the chamber. The torque exerted on the rotating rollers during the mixing process is continuously monitored. This torque is directly linked to the shear stress experienced by the mixer walls and the mixed compound. The procedure begins with the binder being thoroughly softened within the heated chamber of the high-shear mixer. Following this, the metallic powder is introduced into the mixing unit. As the material level within the feeding unit rises, so does the torque. As the metallic powder disperses within the melted binder, both viscosity and torque decrease. The mixing process of the compound reaches a steady state when the torque stabilizes. Once compounding is complete, the mixed compound should be extracted from the mixing chamber while it remains in a molten state and then allowed to cool at room temperature. Following this, the feedstock needs to be mechanically ground to a size of 1–3 mm and then subjected to drying in an oven [101].

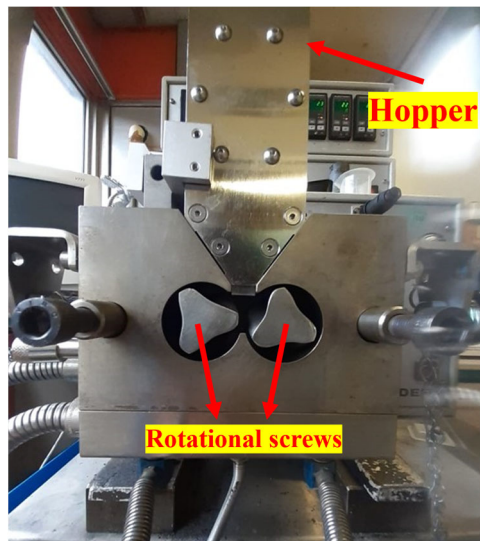


**Figure 3.** Illustration of a kneader or roller mixer designed for small-scale production mixing purposes.

An alternative equipment option for compounding feedstock involves continuous production processes, which can be achieved using co-rotating twin-screw extruders. In this apparatus, both metallic powder and binder pellets are introduced into two gravimetric feeding units. The mixing occurs in the solid state as the materials progress toward the extruder barrel. Subsequently, the twin screws propel the materials into a heated mixing zone, wherein the polymer softens, facilitates wetting, and promotes the uniform mixing of the feedstock under conditions of high shear stress. As the metallic powder disperses within the softened polymer, a consequential decrease in torque is observed. The process is considered finalized when the torque stabilizes at a steady state, indicative of the successful completion of feedstock compounding. In commercial contexts, the twin-screw extruders commonly employed are equipped with 1–11 heating zones, ensuring a thorough and uniform mixing process [101]. Figure 4 shows an example of the extrusion of copper feedstock with co-rotating twin-screw extruders.

Thorough compounding ensures the uniform dispersion of powder particles and binder components throughout the shaping process (MEX printing). If the dispersion within the 3D-printed parts is inhomogeneous, there is a significant probability of encountering irregular shrinkage during debinding and sintering. Additionally, various apparent surface imperfections, such as excessive porosity, cracks, and warping, can manifest in the sintered components [14]. During the compounding stage, the selection of mixing temperature depends on both the thermal stability of the binder systems and the viscosity of the feedstock. It is recommended to use lower temperatures for feedstocks with lower viscosity, while higher temperatures are more suitable for feedstocks with higher viscosity [66].

Following feedstock development, the subsequent phase involves filament extrusion. For large-scale production, single-screw extruders are commonly utilized, whereas capillary rheometers are employed for laboratory-scale fabrication [14]. A schematic representation of the extrusion line for the production of filaments for MEX can be found in Figure 5a. Filament diameter should be carefully monitored for quality and diameter tolerance. Laser micrometers are commonly used for this purpose [75]. Maintaining the recommended filament diameter (e.g.,  $1.75 \pm 0.05$  mm,  $2.85 \pm 0.05$  mm) is crucial to avoid voids or feeding issues in 3D printing. For an example of the appropriate diameter range of the filament spool used in the earlier work [75], see Figure 5b. Low ovality is also important for proper filament grip and continuous feeding, as recommended in the existing literature [66,102]. Furthermore, the suitability of filaments for MEX hinges not solely on filament geometry but also on their mechanical attributes, processing parameters, feedstock flow characteristics, and extruder head design. Generally, material flow properties are highly influenced by

factors such as solid loading, binder behavior, temperature, agglomeration state, and shear rate [13,76,103].

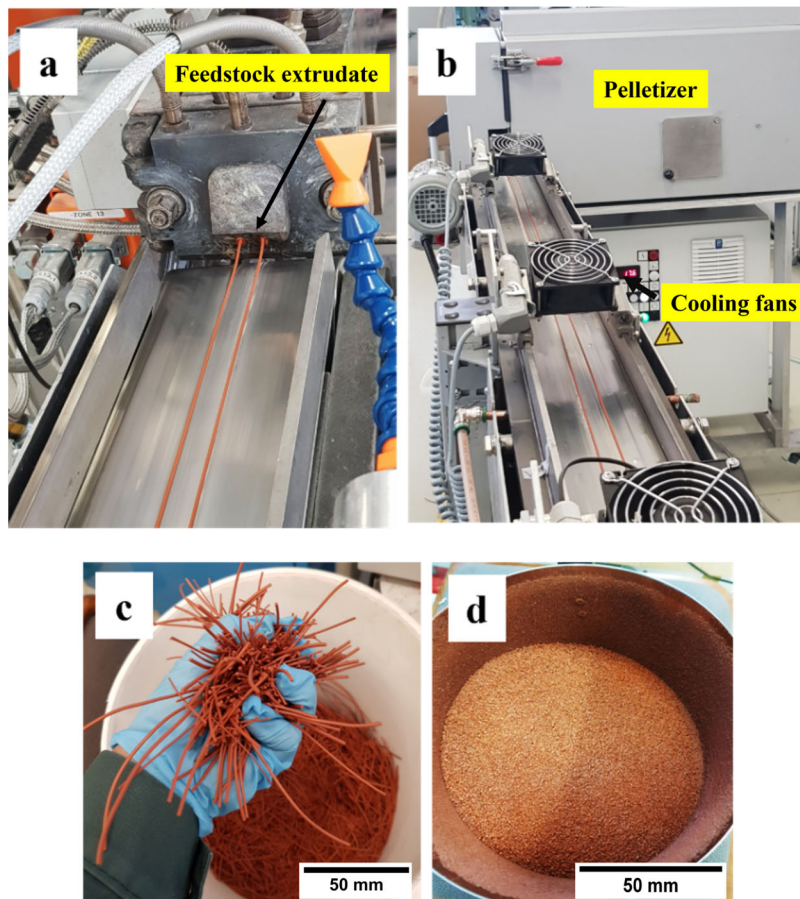


**Figure 4.** (a) The extrusion of copper feedstock using co-rotating twin-screw extruders transported in a conveyor belt; (b) copper feedstock passing under cooling fans to cool down the extrudate and continuous pelletizing through cutting mill; (c) feedstock collected after extrusion in short strands; and (d) feedstock pellets after pelletizing using the cutting mill [46].

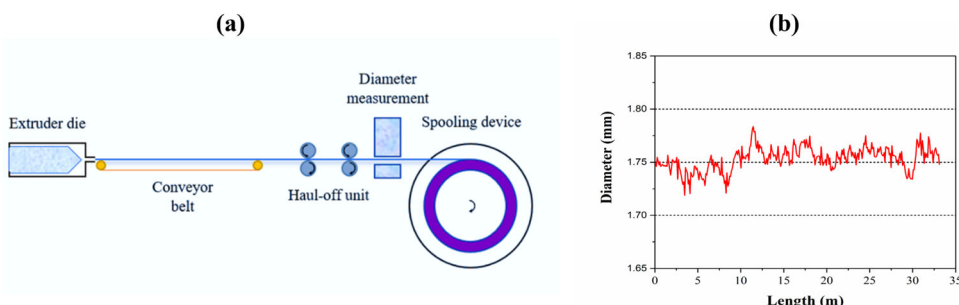


**Figure 5.** (a) A schematic representation of extrusion line in the production of filaments for MEX [46] and (b) the suitable diameter range of the filament spool employed in the production of copper filled MEX specimens [75].

#### 2.4. Shaping

Following filament compounding, the subsequent stage involves shaping, where parts are constructed layer by layer using MEX technology. An outline of the material extrusion process with filaments is depicted in Figure 6a).

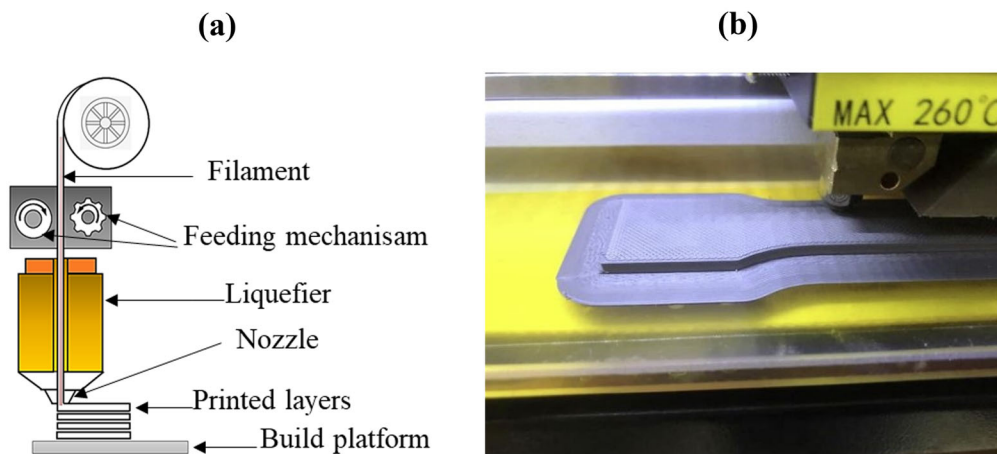


**Figure 6.** (a) A schematic illustration of material extrusion (MEX) with filaments (adapted from [14]) and (b) an example of the MEX printing of stainless steel 316L-based filaments [104].

Firstly, the filament is introduced into the printing machine via a mechanism involving two counter-rotating rollers. This filament progresses into the liquefier section, where it undergoes melting. Essentially, the filament functions as a piston, propelling the molten portion and facilitating its flow through the orifice or nozzle [105]. The material is heated to a temperature slightly above its melting point, such as in the case of semi-crystalline polymers, or well above the glass transition temperature, in the case of amorphous polymers [106]. The extruder head's temperature exceeds that of the building plate, causing the material to solidify upon contact with the latter. Generally, the printing bed temperature ranges from 70 to 120 °C, depending on the material. This controlled heating aids in enhancing layer adhesion and minimizing material warping [3,21]. The initial layer deposited onto the building platform holds great significance for the outcome of the part. Adequate adhesion during melting is crucial, as poor adhesion could lead to heightened warping or printing failure, as reported by Sadaf et al. (Figure 7a,b) [5].



**Figure 7.** (a,b) An example of printing failure due to unwanted warpage [46].

The result of extrusion-based 3D printing using metal/ceramic powder–binder mixtures is typically referred to as the “green body.” The shaping of metal feedstock through MEX has been documented in the existing literature. For an overview of different MEX machine models used with various feedstocks, refer to Table 3.

**Table 3.** Equipment used to process metallic feedstocks for MEX.

MEX Model (Filament-Based)	Fillers in Feedstock	Refs.
Wanhao Duplicator i3 v2	Stainless steel 316L, stainless steel, 17-4PH, copper	[67,74,96]
Ultimaker 2	Stainless steel 316L	[107]
Hage3D-72L	Stainless steel 316L, stainless steel 17-4PH	[98,108]
FLM printer X1000	Stainless steel 316L, copper	[62]
Pulse 3D printer	Titanium (Ti-6Al-4V)	[80]
Prusa i3 MK2	Titanium (Ti-6Al-4V), stainless steel 316L	[81]
Renkforce 1000 3D printer	Titanium (Ti-6Al-4V)	[83]
Renkforce 2000 3D printer	Stainless steel 17-4PH	[68]
Hage3D-140L	Rare-earth magnets (NdFeB)	[86]
Stratasys FDMTM	Tungsten carbide–cobalt	[66]
Fused deposition of metals (FDMet)	Stainless steel 17-4PH, carbonyl iron, tungsten carbide–cobalt	[65,66,85]
Flashforge Dreamer	Stainless steel 316L	[61]
L-DEVO M2030TP	Stainless steel 316L	[43]
Apium P155	Stainless steel 316L	[59]
Zortrax M200	Stainless steel 316L	[63]

Numerous investigations have explored the influence of various printing parameters on the characteristics of green printed components using MEX. These studies have revealed that factors such as temperature, raster angle, printing speed, and infill density, among others, exert a significant impact on the bonding between deposited layers and consequently affect the mechanical properties of the final MEX-based printed items [109–111]. Elevating the temperatures of both the nozzle and the print bed has been observed to enhance adhesion between adjacent layers. This improvement is attributed to the increased mobility of polymeric chains, promoting greater inter-diffusion among the strands. Such strong adhesion serves as a barrier against unwanted defects, like voids or pores, resulting in superior mechanical properties [46]. Figure 8 shows an example of various metal-filled green parts produced using extrusion-based additive manufacturing.

Another critical printing parameter is the extrusion multiplier (flow rate), which demands careful selection depending on the material in use. The extrusion multiplier determines the quantity of material passing through the nozzle, with 100% representing the standard flow rate. A higher extrusion multiplier (>100%) ensures a more robust flow rate, leading to improved deposition of the extruded material, reduced printing voids, and enhanced adhesion with the perimeter layer [14,112]. This heightened flow rate contributes to lower porosity, thereby enhancing green density. Furthermore, increasing the flow multiplier reduces surface roughness. Conversely, a lower extrusion multiplier results in inadequate deposition of extruded material, leading to the formation of large surface voids and an unsatisfactory surface finish.

The printing speed also plays a significant role in shaping the morphology of the extruded material [46,75,112]. Sadaf et al. [75] reported that lowering the printing speed enhanced surface quality due to more consistent extruded material shape. Conversely, higher speeds increased the volumetric flow through the nozzle, causing greater pressure drops and leading to rougher surfaces and deformed edges in the printed specimens. Regarding green density, higher nozzle speeds promote improved inter-layer bonding with minimal extrusion voids. This is a result of the reduced time between the deposition of successive layers, which mitigates the cooling of the deposited material and enhances bonding.



**Figure 8.** Example of various metal-filled green parts through extrusion-based additive manufacturing, demonstrating superior quality and shape adaptability: (a) stainless steel 316L; (b) stainless steel 17-4PH; (c) Ti6Al4V; (d) NdFeB; (e) YSZ; and (f) YSZ and stainless steel 17-4PH [113].

### 2.5. Debinding

Debinding constitutes a crucial phase in 3D printing, wherein the binder components are selectively removed from the printed parts while preserving the original compact's shape. This step ranks among the most pivotal but time-consuming aspects of post-processing. Traditionally, binder removal is accomplished with solvent and/or thermal debinding methods. Additionally, an industrial-scale technique known as catalytic debinding has gained prominence [14,90]. Following the successful elimination of the binder, the resulting product is referred to as a "brown part". This article proceeds to elaborate on these three debinding techniques in greater detail [14,50,114]:

- Solvent debinding: This method involves immersing green parts in liquid or gaseous solvents, such as heptane, ethanol, acetone, and hexane, among others. Typically, a temperature range of 50–70 °C is applied, depending on the specific solvent used. The fundamental principle behind this process is that MEX-printed components can be introduced into an environment saturated with a solvent. Subsequently, the primary binder within the component undergoes a phase change, transitioning from a solid to a liquid state, and is thus removed from the component structure. This action effectively opens a network of pores, facilitating the subsequent removal of the backbone binder during the thermal debinding stage [60,115]. It is crucial to ensure compatibility between the solvent and the binder material for successful solvent debinding. Additionally, the debinding time is significantly influenced by the thickness of the MEX-printed component, with thicker components and smaller particle sizes requiring longer removal times. Critical parameters in the debinding process encompass the selection of an optimal temperature for solvent debinding. Excessively low temperatures may induce rapid solvent diffusion within the green compact, resulting in the swelling of the green part. Consequently, this swelling can cause pronounced internal stress within the component, ultimately culminating in the formation of cracks. Conversely, excessively high temperatures pose the risk of green component collapse due to the softening of the binder material [50,90,93].
- Thermal debinding: This technique is based on the thermal degradation of the binders. The components should be placed inside the debinding furnace, and the temperature

should be increased up to the evaporation temperature of the polymer materials used. Once the evaporation temperature is reached, the ramping temperature is set on hold for a certain time until the whole polymer is decomposed. Polymer removal through thermal debinding involves chemical and physical methods. The chemical process occurs due to thermal degradation based on the continuous dissociation of polymers to generate low-molecular-weight volatile products. The physical process involves the diffusion of volatile products onto and out of the surface of the component [101]. Compact heating depends on heat transfer and the reaction enthalpies correlated with the dissociation of polymeric chains, leading to thermal-kinetic results that link to the chemical-physical aspects. The degradation temperature and time are dependent on the nature of the polymer used and its thermal conductivity [48,116].

- Catalytic debinding: This method combines both solvent and thermal debinding mechanisms, primarily relying on the catalytic action of acids to remove the binder. During this process, catalytic acids play a pivotal role in initiating the dissociation of polymeric chains within the material. These catalysts are specifically designed to lower the temperature at which the polymeric chains break down. Typically, the debinding chamber contains a controlled concentration of catalytic acid vapor, with nitric acid being a commonly employed catalyst. Nitrogen gas is often introduced to prevent oxidation during the process [48]. Catalytic debinding is known for its relative efficiency and speed compared with other debinding techniques. However, it is worth noting that this method is not universally applicable to all metals, posing a significant limitation. Some metals may risk contamination or corrosion during catalytic debinding, underscoring the need for careful selection of the appropriate acid to safeguard equipment integrity. Catalytic debinding finds extensive use in the powder injection molding (PIM) industry, with polyoxymethylene (POM) serving as a notable example, as it undergoes decomposition under the influence of acid attack [101].

Complete removal of the binder material is imperative prior to the final sintering phase, as inadequate binder elimination can result in the formation of flaws detrimental to the quality of the sintered components [50]. Numerous factors contribute to incomplete binder removal, with particular significance being attached to factors such as incorrect debinding temperatures, inappropriate heating rates, and/or insufficient holding durations [14]. Notably, rapid heating rates often lead to thermal debinding defects, primarily stemming from the swift decomposition of the binder constituents. Conducting a thermogravimetric analysis (TGA) on the feedstock offers a dependable means of assessing the polymer's thermal stability and its associated degradation temperature. Furthermore, the utilization of scanning electron microscopy (SEM) proves advantageous for investigating the morphological transformations exhibited by the debound components. This approach enables the exploration of the relation between binder burnout and the distribution of pore sizes, thus offering insights into the efficacy of the debinding process [58].

## 2.6. Sintering

Following the debinding process, sintering should be performed. Sintering represents a thermal treatment conducted at approximately 90% of the metal powder's melting point, aimed at consolidating and bonding the loose particles to form a dense, cohesive structure [117]. Within this sintering phase, powder particles establish cohesive bonds and undergo densification through pore size reduction.

Sintering diminishes the surface energy of the powder mass through the formation of inter-particle bonds, subsequently leading to a decrease in surface area. This reduction in the overall interfacial area of the powder compact can be quantified as follows [118]:

$$\Delta(\gamma A) = \Delta\gamma A + \gamma\Delta A \quad (1)$$

where “A” represents the overall surface area, “ $\gamma$ ” denotes the specific surface area, “ $\Delta A$ ” signifies the alteration in surface area attributed to grain growth (grain coarsening), and “ $\Delta\gamma$ ” accounts for the change in interfacial energy, which arises from densification. Densification pertains to the transition from vapor/solid surfaces to solid/solid surfaces during solid-state sintering [118].

As inter-particle coherent bonding grows, significant alterations arise within the pore structure, resulting in notable improvements in various essential properties. These enhancements encompass ductility, strength, electrical conductivity, magnetic permeability, and corrosion resistance. These transformations hold paramount significance in various industrial applications, including but not limited MEX-based additive manufacturing, powder metallurgy (PM), and metal/ceramic injection molding (MIM/CIM) [48].

### 2.6.1. Mass Transport Mechanisms

The natural vibration and movement of atoms combined with nature’s need to eliminate free surfaces to minimize surface energy leads to the development of inter-particle coherent bonds. Additionally, elevated temperatures intensify this process. Simultaneously, the gradual elimination of free surfaces initiates pore mobility, facilitated by the movement of vacancies traversing grain boundaries as conduits. Furthermore, the reduction in grain boundaries through grain growth contributes to a reduction in energy. As the sintering process progresses, a cascade of mass transport mechanisms within the particles becomes active, collectively referred to as the bulk transport mechanism. These mass transport mechanisms encompass grain boundary diffusion, surface diffusion, viscous flow, lattice diffusion, plastic flow, and evaporation–condensation processes [48,101,119,120].

Diffusion is an important temperature-dependent mechanism of sintering. The diffusion coefficient ( $D$ ) can be expressed as [118]

$$D = D^\circ \exp\left(-\frac{Q}{RT}\right) \quad (2)$$

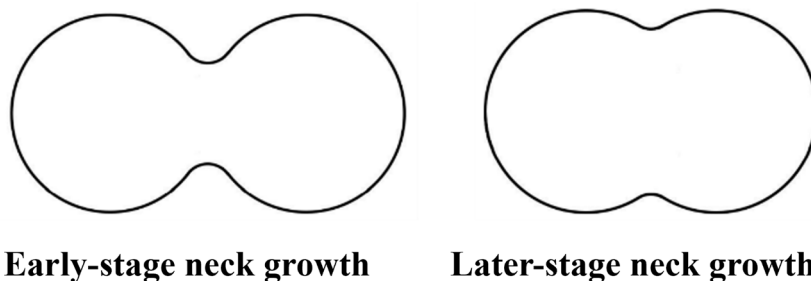
where “ $D$ ” is a diffusion coefficient expressed in  $\text{cm}^2/\text{s}$ , “ $D^\circ$ ” is a constant expressed in  $\text{cm}^2/\text{s}$ , “ $R$ ” is the universal gas constant (8.314 J/mol), “ $Q$ ” is the activation energy (in J/mol), and “ $T$ ” is the absolute temperature (expressed in K) [118].

### 2.6.2. Stages of Sintering

There are three stages of sintering, which are explained step by step below [47,48,119,121]:

1. Neck formation: This initial sintering stage marks the onset of particle-to-particle interactions and the simultaneous smoothing of the particles’ free surfaces. At this point, the formation of “necks” at interaction points is driven by mass transport mechanisms, including evaporation–condensation, surface diffusion, and volume diffusion (Figure 9). A modest degree of shrinkage occurs in this early phase. Following the establishment of these necks, the compaction of the material experiences an increase of up to 3% in density. This progression is notably rapid due to the exposure of the powder to elevated temperatures, owing to the elevated surface area and the pronounced driving force promoting sintering.
2. Densification: During this phase, with increasing temperatures, the necks between particles undergo expansion owing to the influence of various mass transport mechanisms (Figure 10). These mechanisms encompass grain boundary diffusion, surface diffusion, viscous flow, lattice diffusion, plastic flow, and evaporation–condensation processes. Furthermore, the porosity within the component diminishes as sintering progresses.
3. Grain growth: This represents the final stage in the sintering process, commencing when the material reaches approximately 93–95% of its theoretical density, as most of the porosity has already been isolated. In an ideal scenario, by the conclusion of this phase, all remaining porosity is eliminated. The complete eradication of

porosity during the last stage of sintering is achievable only when all pores are either interconnected or follow distinct, unobstructed diffusion pathways along grain boundaries. Such favorable conditions take place only if the pores go along with the direction of the grain boundaries and do not stay within the grains. However, if sintering is excessively prolonged, grain size may undergo enlargement, which can subsequently lead to a decline in mechanical properties.



**Early-stage neck growth      Later-stage neck growth**

**Figure 9.** The initial stage in progression of sintering [47,48].

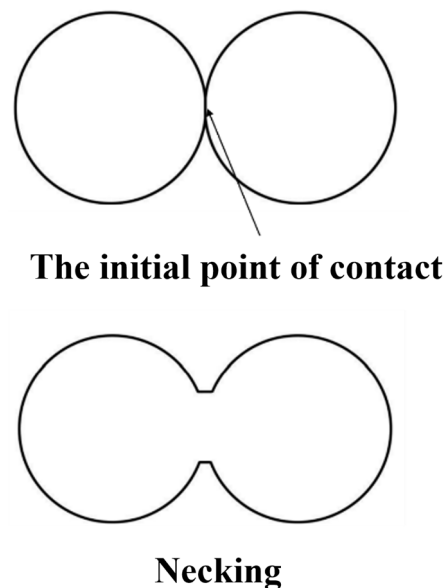


**Figure 10.** Intermediate stage in progression of sintering [47,48].

### 2.6.3. Sintering Parameters

The most critical factors from a practical standpoint in the sintering process are sintering temperature and time. Additionally, there are other relevant parameters that play a role, such as the heating and cooling rates and the atmosphere during sintering, as well as particle size and geometry [122].

When the sintering temperature and holding time are increased, the porosity of the material decreases, leading to improved density. However, this can also cause an increase in grain size, which in turn affects the material's hardness and mechanical strength. Notably, research has shown that sintering temperature has a more significant impact on grain size compared with sintering time [73].

Proper sintering is crucial to obtaining parts with desirable mechanical properties and corrosion resistance. Inadequate sintering results in inferior mechanical properties, as well as low corrosion resistance. Signs of insufficient sintering include poor bonding; retention of original particle boundaries; the presence of sharp pores; and a high concentration of interstitials, like carbon and oxygen [123].

The cooling rate during the sintering process also influences the mechanical properties. Effective control of the cooling rate, particularly from the sintering temperature to approxi-

mately 500 °C, is vital to preventing issues like re-oxidation, carbide formation, and nitride formation, all of which can negatively impact ductility and corrosion resistance [124].

#### 2.6.4. Sintering Atmosphere

Every metal is susceptible to oxidation to some degree, and it is imperative to prevent oxidation, as it can detrimentally impact the structural properties of metals. Oxidation primarily takes place at the exposed surfaces of the material. The sintering process, which involves high temperatures, can facilitate and induce oxidation reactions. It is noteworthy that metal components produced through MEX and MIM are particularly sensitive to oxidation during their production, with sintering being a critical stage in this regard [48,50,92,116].

To safeguard metal components from oxidation during sintering, it is imperative to maintain an oxygen-free atmosphere. This can be achieved by purging the sintering furnace of all oxygen and replacing it with a less reactive gas, such as hydrogen or nitrogen. The selection of the sintering atmosphere should be meticulous and tailored to the reactivity of the specific metals being processed. For instance, titanium, known for its extreme reactivity, reacts even with nitrogen during sintering. Consequently, sintering procedures for titanium typically take place in an argon atmosphere or in a vacuum environment. Argon, known for its inert nature, is a preferred choice for sintering highly reactive metals in general [48,119]. When sintering stainless steel, hydrogen is a highly favored choice, as it serves as a reductant and undergoes oxidation itself instead of the metal component. Moreover, the hydrogen atmosphere serves to prevent redox reactions between carbon and chromium. Thus, selecting the appropriate atmosphere, alongside other sintering parameters, is crucial to controlling the structural properties of metals [48].

#### 2.6.5. Shrinkage and Densification

The shrinkage observed in MEX-shaped metal components primarily arises from densification and the reduction in porosity. Previous literature reports [125,126] have noted that this shrinkage does not occur uniformly across all dimensions. In the case of parts produced through MIM, there is a predominant occurrence of anisotropic shrinkage, primarily attributed to polymer alignment. These alignments exert a significant influence on the parameters of MIM [127,128]. Conversely, for MEX-shaped metal parts [86], the density and shrinkage can be influenced by the presence of substantial gaps between the printed layers. Notably, larger gaps are unable to be closed during the sintering process. As an example [68], Figure 11 shows 3D-printed components made of stainless steel 17-4PH before and after sintering.

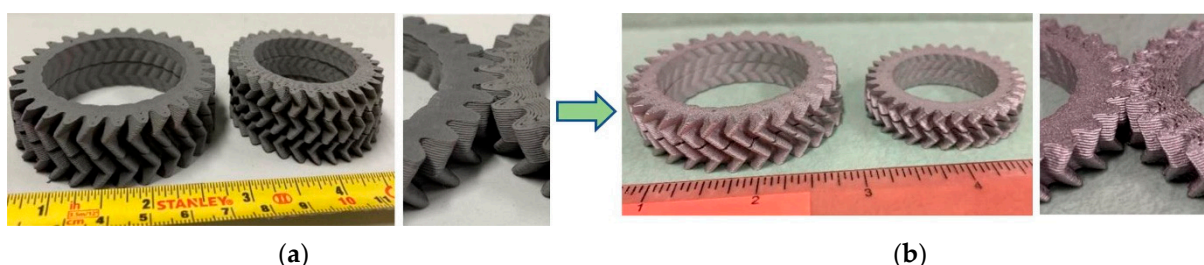


**Figure 11.** Three-dimensionally printed stainless steel 17-4PH components: (a) green and (b) sintered, which represents clear shrinkage [68].

The dimensional changes resulting from sintering can be anticipated by taking into account the shrinkage factor ( $\gamma$ ). This shrinkage factor ( $\gamma$ ) is determined by considering the material's theoretical density, the solids loading of the feedstock, and the ultimate density of the component. The shrinkage factor can be computed using the following formula [48]:

$$\gamma = 1 - \left( \frac{\rho}{\rho_t} \right)^{1/3} \quad (3)$$

where “Y” is the shrinkage factor (expressed in %), “ $\emptyset$ ” is the feedstock solids loading, “ $\rho$ ” is the final density (expressed in  $\text{g cm}^{-3}$ ), and “ $\rho_t$ ” is the theoretical density (expressed in  $\text{g cm}^{-3}$ ) [48].

Table 4, reporting the previous literature, contains information regarding the density and linear shrinkage observed in components fabricated using MEX following the sintering process.

**Table 4.** Density and linear shrinkage of MEX of metals.

Material	Linear Shrinkage (%)	Density (%)	Ref.
Stainless steel (316L)	19.2 ± 0.02	95–98	[14,59,61]
Stainless steel (316L)	N.A.	92–95	[62]
Stainless steel (316L)	17–20	N.A.	[63]
Stainless steel (17-4PH)	16–20.3	N.A.	[64]
Stainless steel (AISI 630)	12.1	N.A.	[69]
Stainless steel (17-4PH)	16–20.3	N.A.	[64]
Stainless steel (AISI 630)	12.1	N.A.	[69]
Copper	20–21	90	[73]
Copper	16–17.5	N.A.	[74]
Copper	N.A.	80	[62]
Titanium (Ti-6Al-4V)	15	90–93	[81]
Titanium (Ti-6Al-4V)	14	94.1	[56]
Titanium (Ti-6Al-4V)	N.A.	92–99.1	[82]
Titanium (Ti-6Al-4V)	N.A.	91	[83]
Rare-earth magnets (NdFeB)	17.8–19.3	94.5–96.5	[86]

### 3. Comparison of MEX and Other Manufacturing Processes

The cost effectiveness, short production time, minimal carbon emissions, and ease of operation of MEX machinery have spurred its widespread adoption in both industrial and consumer settings for the production of polymeric components. Furthermore, this technique offers the distinct advantage of directly manufacturing final products without the need for tooling, dies, or molds, which are significant limitations of conventional manufacturing processes [9,129]. The popularity of MEX, along with the existing knowledge base, holds the potential to drive its application and growth in the production of ceramic and metal materials. Several 3D printer development companies are actively promoting the use of MEX for metal printing. For instance, Desktop Metal has commenced the sale of commercial systems that incorporate a streamlined one-step debinding and sintering process [130]. Additionally, the complete setup for shaping, debinding, and sintering can now be obtained for a few thousand euros (EUR) [129].

The processes of debinding and sintering have gained considerable recognition in the realm of established manufacturing techniques, like powder injection molding (PIM). In light of these considerations, this approach can complement material extrusion (MEX) as a parallel manufacturing method, suitable for small-batch production, new-product development, tooling manufacturing, production of intricate geometric components, and customization of mass-produced parts [1,4,131]. Typically, most commercial MEX machines are equipped with a single extrusion head. However, contemporary MEX machines have advanced their capabilities by offering the flexibility to incorporate two or more extrusion heads, enabling simultaneous use of different materials or colors within the same object or layer (3D multi-material fabrication) [3,19,22]. Another avenue for expanding the capabilities of MEX machines involves the development of larger building chambers. These larger chambers offer the advantage of accommodating the production of larger green components, setting MEX apart from other manufacturing methods, such as material or binder jetting and vat photopolymerization [131].

MEX encounters primary limitations concerning its surface finishing, which tends to be less refined compared with traditional manufacturing techniques [61]. One approach to minimize surface roughness involves using nozzles with smaller diameters, as they

enable the deposition of thinner layers, thus enhancing surface quality. Furthermore, surface roughness exhibits an inverse relationship with layer thickness, meaning that optimization of layer thickness can minimize roughness [51]. Another limitation pertains to the size of the printable components. Safkta et al. [132], in their work on producing 316L stainless steel MEX components, demonstrated that this issue is linked not to the printing process but, rather, to post-processing. During thermal debinding and sintering, specimens with walls with very high thickness exhibited cracks and other defects. In the overall processing of MEX components, the most critical stage is debinding. When employing a single-step thermal debinding process, it necessitates expensive and lengthy thermal cycles to prevent defects in the components. In the context of ceramic vat photopolymerization, thermal debinding stands as the sole option for removing the binder from the fabricated components [133].

The mechanical characteristics of sintered components produced through MEX are typically inferior to those achieved using alternative manufacturing techniques like SLM, MIM, and SLS. A comparative assessment of the mechanical properties of MEX-produced 316L stainless steel in comparison to other technologies is provided in Table 5. This disparity in mechanical properties can be primarily attributed to the presence of porosity in the final MEX products compared with other techniques. Carminati et al. [134,135] demonstrated the attainment of a notable 95% relative density in MEX-based 316L stainless steel, accompanied by optimal shrinkage and commendable dimensional stability. Despite these successes, the final metallic components exhibited lower ultimate tensile strength (UTS) and yield strength due to process-induced stress. In addition, phase analysis revealed the presence of  $\delta$ -ferrite in the austenitic matrix, offering insights into the brittleness of the MEX metal specimens. Gong et al. [136] found that Ultrafuse 316L stainless steel produced with MEX exhibited remarkable ductility, achieving 20% elongation without rupture; however, its lower yield strength, UTS, modulus of elasticity, and hardness compared with flat-rolled 316L stainless steel are attributed to grain size and an austenitic microstructure, and the isotropic microstructure shows consistent hardness values in both the horizontal and vertical printing directions, confirming the dislocation-free nature of components printed with MEX. Pellegrini et al. [137] and Spiller et al. [138] reported on the reduction in the mechanical properties of MEX 316L stainless steel due to process-induced porosity.

MEX-based components are well suited for prototyping and visualization, although porosity and the need for improved mechanical properties limit the industrial use of this technology to non-critical, high-value metal parts, such as corrosion-resistant tanks and pipelines in the chemical industry [135]. For non-structural purposes, the material's biocompatibility makes it suitable for the food industry and medical sector, and its ability to form intricate shapes extends its use to heat exchangers and heat sinks [135].

However, careful control of printing and sintering parameters, particularly sintering temperature, can yield improvements in the mechanical properties of MEX end products [47,48,116]. To enhance the mechanical properties of MEX products, post-processing thermal treatments (e.g., quenching) or cold working techniques (e.g., shot peening) can be employed to modify either the grain size or the microstructure [139,140]. Damon et al. [59] demonstrated impressive mechanical properties and achieved a relative density of approximately 99.5% using controlled build direction and printing strategies, highlighting the potential applications of MEX-based metal components. In addition, intensive research is currently underway to improve the mechanical properties of MEX components in order to expand the application range of this technology [135].

**Table 5.** The mechanical properties of MEX-produced 316L stainless steel in comparison to other additive manufacturing (AM) and conventional methods.

Process	Yield Strength (MPa)	Tensile Strength (MPa)	Elastic Modulus (Gpa)	Densification (%)	Ref.
MEX	167	465	152	98.5	[61]
MEX	234–251	521–561	n.d.	n.d.	[44]
MEX	500	900	n.d.	95	[60]
MEX	155–165	500–520	210	98.3–99.5	[59]
MEX	167	436	n.d.	n.d.	[136]
MEX	125–161	405–464	n.d.	~95.3	[134]
MEX	~130	~460	150–230	n.d.	[137]
MEX	139–161	441–473	172–203	n.d.	[138]
MIM	170–205	460–560	n.d.	98.5	[141]
MIM	n.d.	527–590	n.d.	97.7–99.1	[142]
DED	405–415	620–720	n.d.	n.d.	[143]
DED	580	900	n.d.	n.d.	[144]
SLM	590	700	227.3	> 99	[61]
SLM	208.8–469.6	486.4–644.3	141–205	> 99.3	[145]
PBF	450–525	620–650	n.d.	99	[146]
PBF	400–420	550–580	180–202	98	[147]
BJ	n.d.	700–780	n.d.	n.d.	[148]
BJ	214	517	n.d.	98.7	[118]
Hot rolling	n.d.	585	245	n.d.	[149]
Flat rolling	170	485	n.d.	n.d.	[136]
Cast	n.d.	575	288	n.d.	[150]

#### 4. Conclusions

In conclusion, this review has provided a comprehensive overview of the current state of material extrusion as a promising approach to the additive manufacturing of metal components. We have explored the key principles, techniques, post-treatment, and materials used in this technology, highlighting its advantages, such as cost effectiveness, versatility, and ease of use. Through a thorough analysis of the existing literature, we have also discussed the challenges and limitations that researchers and manufacturers face when implementing material extrusion for metal additive manufacturing. These challenges encompass issues related to surface finish and post-processing requirements. Despite these challenges, the research community has made significant strides in addressing them and enhancing the capabilities of material extrusion in the metal AM domain.

#### 5. Research Outlook

The future of material extrusion in metal additive manufacturing holds immense promise and potential. With ongoing research and development efforts, we are on the verge of transformative advancements. We anticipate the emergence of novel, high-performance metal filaments and powders that will elevate the capabilities of material extrusion. Process optimization will continue to refine the art of metal 3D printing, ensuring smoother prints, enhanced mechanical properties, and superior surface finishes. Standardization and rigorous quality assurance practices are poised to cement the technology's reliability, while sustainability considerations will make it a responsible choice for industries. As

material extrusion for metal additive manufacturing continues to mature, it promises to revolutionize manufacturing practices, offering innovative, cost-effective solutions across diverse sectors.

**Author Contributions:** Conceptualization, M.S. and F.N.; validation, M.S., M.B. and F.N.; visualization M.S.; resources, F.N.; writing—original draft preparation, M.S.; writing—review and editing, M.S., M.B., F.N. and L.S.P.; supervision, M.B. and F.N.; project administration, M.S.; funding acquisition, F.N. and L.S.P. All authors have read and agreed to the published version of the manuscript.

**Funding:** The authors sincerely appreciate the support from Slovenian Research Agency (research core funding No. P2-0264).

**Institutional Review Board Statement:** Not applicable.

**Data Availability Statement:** Data are contained within the article.

**Acknowledgments:** The authors extend their gratitude to Muhammad Shoaib Naseem Siddiqui for his valuable assistance in creating visual schematic diagrams.

**Conflicts of Interest:** The authors declare no conflicts of interest.

## References

1. Riecker, S.; Hein, S.; Studnitzky, T. 3D Printing of Metal Parts by Means of Fused Filament Fabrication—A Non Beam-Based Approach. In Proceedings of the EuroPM 2017—AM Alternative Technologies, Milan, Italy, 1–5 October 2017.
2. Andersen, O.; Riecker, S.; Studnitzky, T.; Hein, S.; Lohse, U.; Kie, B. Manufacturing and Properties of Metal Parts Made by Fused Filament Fabrication. *Powder Metall.* **2018**, *18*, 2–7.
3. Masood, S.H. Advances in Fused Deposition Modeling. In *Comprehensive Materials Processing*; Elsevier B.V: Amsterdam, The Netherlands, 2014; Volume 10, pp. 69–91, ISBN 9780080965338.
4. Gao, W.; Zhang, Y.; Ramanujan, D.; Ramani, K.; Chen, Y.; Williams, C.B.; Wang, C.C.L.; Shin, Y.C.; Zhang, S.; Zavattieri, P.D. The Status, Challenges, and Future of Additive Manufacturing in Engineering. *CAD Comput. Aided Des.* **2015**, *69*, 65–89. [[CrossRef](#)]
5. Turner, B.N.; Strong, R.; Gold, S.A. A Review of Melt Extrusion Additive Manufacturing Processes: I. Process Design and Modeling. *Rapid Prototyp. J.* **2014**, *20*, 192–204. [[CrossRef](#)]
6. Belei, C.; Meier, B.; Amancio-Filho, S.T. Manufacturing of Metal&ndash;Polymer Hybrid Parts Using a Desktop 3-Axis Fused Filament Fabrication 3D-Printer. *Metals* **2023**, *13*, 1262. [[CrossRef](#)]
7. Podmiljsak, B.; Kobe, S.; Tomše, T.; Bek, M.; Kotnik, T.; Slemenik Perše, L.; Žagar, E.; Saje, B.; Žužek, K.; Šturm, S. Additive-Manufactured Anisotropic Magnets for Harsh Environments. *J. Magn. Magn. Mater.* **2023**, *586*, 171165. [[CrossRef](#)]
8. Ramazani, H.; Kami, A. Metal FDM, a New Extrusion-Based Additive Manufacturing Technology for Manufacturing of Metallic Parts: A Review. *Prog. Addit. Manuf.* **2022**, *7*, 609–626. [[CrossRef](#)]
9. Smith, W.C.; Dean, R.W. Structural Characteristics of Fused Deposition Modeling Polycarbonate Material. *Polym. Test.* **2013**, *32*, 1306–1312. [[CrossRef](#)]
10. Rane, K.; Strano, M. A Comprehensive Review of Extrusion-Based Additive Manufacturing Processes for Rapid Production of Metallic and Ceramic Parts. *Adv. Manuf.* **2019**, *7*, 155–173. [[CrossRef](#)]
11. Zhou, W.; Lin, J.; Dean, T.A. Microstructure and Mechanical Properties of Curved AZ31 Magnesium Alloy Profiles Produced by Differential Velocity Sideways Extrusion. *J. Magnes. Alloy.* **2023**, *11*, 493–508. [[CrossRef](#)]
12. Zhang, Z.; Zhou, W.; Shi, Z.; Lin, J. Investigation of Die Designs on Welding Quality and Billet Material Utilisation for Multi-Container Extrusion of Wide Stiffened Aluminium Panels. *Int. J. Adv. Manuf. Technol.* **2023**, *127*, 4149–4162. [[CrossRef](#)]
13. Bragaglia, M.; Sadaf, M.; Rinaldi, M.; Nanni, F. PEEK-Titanium Dioxide 3D Printable Filaments: Influence of TiO<sub>2</sub> on UV Resistance. In Proceedings of the ECNP Congress, San Sebastian, Spain, 3–5 October 2018; p. 1.
14. Gonzalez-Gutierrez, J.; Cano, S.; Schuschnigg, S.; Kukla, C.; Sapkota, J.; Holzer, C. Additive Manufacturing of Metallic and Ceramic Components by the Material Extrusion of Highly-Filled Polymers: A Review and Future Perspectives. *Materials* **2018**, *11*, 840. [[CrossRef](#)] [[PubMed](#)]
15. Quarto, M.; Giardini, C. Additive Manufacturing of Metal Filament: When It Can Replace Metal Injection Moulding. *Prog. Addit. Manuf.* **2023**, *8*, 561–570. [[CrossRef](#)]
16. Singh, N.; Siddiqui, H.; Koyalada, B.S.R.; Mandal, A.; Chauhan, V.; Natarajan, S.; Kumar, S.; Goswami, M.; Kumar, S. Recent Advancements in Additive Manufacturing (AM) Techniques: A Forward-Looking Review. *Met. Mater. Int.* **2023**, *29*, 2119–2136. [[CrossRef](#)]
17. Tedla, G.; Rogers, K. Characterization of 3D Printing Filaments Containing Metal Additives and Their Particulate Emissions. *Sci. Total Environ.* **2023**, *875*, 162648. [[CrossRef](#)] [[PubMed](#)]
18. Stratasys Wepbage. 2016. Available online: <http://www.stratasys.com/> (accessed on 20 October 2016).
19. Edgar, J.; Tint, S. Additive Manufacturing Technologies: 3D Printing, Rapid Prototyping, and Direct Digital Manufacturing, 2nd Edition. *Johnson Matthey Technol. Rev.* **2015**, *59*, 193–198. [[CrossRef](#)]

20. Pepelnjak, T.; Stojšić, J.; Sevšek, L.; Movrin, D.; Milutinović, M. Influence of Process Parameters on the Characteristics of Additively Manufactured Parts Made from Advanced Biopolymers. *Polymers* **2023**, *15*, 716. [CrossRef] [PubMed]
21. Carneiro, O.S.; Silva, A.F.; Gomes, R. Fused Deposition Modeling with Polypropylene. *Mater. Des.* **2015**, *83*, 768–776. [CrossRef]
22. Chua, C.K.; Leong, K.F. *3D Printing and Additive Manufacturing State of the Industry, Annual Worldwide Progress Report*; Wohlers Associates: Fort Collins, CO, USA, 2017.
23. Valkenaers, H.; Vogeler, F.; Ferraris, E.; Voet, A.; Kruth, J.-P. A Novel Approach to Additive Manufacturing: Screw Extrusion 3D-Printing. In Proceedings of the 10th International Conference on Multi-Material Micro Manufacture, San Sebastian, Spain, 8–10 October 2013; pp. 235–238.
24. Campbell, I.; Wohlers, T. Markforged: Taking a Different Approach to Metal Additive Manufacturing. Metal AM [Online]. Available online: <https://www.metal-am.com/wp-content/uploads/sites/4/2017/06/MAGAZINE-Metal-AM-Summer-2017-PDF-sp.pdf> (accessed on 11 July 2017).
25. Schuh, C.A.; Myerberg, J.S.; Fulop, R.; Chiang, Y.-M.; Hart, A.J.; Schroers, J.; Vereminski, M.D.; Mykulowycz, N.; Shim, J.J.; Fontana, R. Methods and Systems for Additive Manufacturing. International Patent PCT/US2016/067378, 30 June 2016.
26. Martínez-Vázquez, F.J.; Pajares, A.; Miranda, P. A Simple Graphite-Based Support Material for Robocasting of Ceramic Parts. *J. Eur. Ceram. Soc.* **2018**, *38*, 2247–2250. [CrossRef]
27. Cesarano, J. A Review of Robocasting Technology. *Mater. Res. Soc. Symp. Proc.* **1999**, *542*, 133–139. [CrossRef]
28. Gibson, I.; Rosen, D.W.; Stucker, B. Additive Manufacturing Technologies. In *Rapid Prototyping to Direct Digital Manufacturing*; Springer International Publishing: Berlin, Germany, 2010; pp. 406–407.
29. Bose, A.; Schuh, C.A.; Tobia, J.C.; Tuncer, N.; Mykulowycz, N.M.; Preston, A.; Barbati, A.C.; Kernan, B.; Gibson, M.A.; Krause, D.; et al. Traditional and Additive Manufacturing of a New Tungsten Heavy Alloy Alternative. *Int. J. Refract. Met. Hard Mater.* **2018**, *73*, 22–28. [CrossRef]
30. Bankapalli, N.K.; Gupta, V.; Saxena, P.; Bajpai, A.; Lahoda, C.; Polte, J. Filament Fabrication and Subsequent Additive Manufacturing, Debinding, and Sintering for Extrusion-Based Metal Additive Manufacturing and Their Applications: A Review. *Compos. Part B Eng.* **2023**, *264*, 110915. [CrossRef]
31. Bellini, A.; Shor, L.; Guceri, S.I. New Developments in Fused Deposition Modeling of Ceramics. *Rapid Prototyp. J.* **2005**, *11*, 214–220. [CrossRef]
32. Drescher, P.; Lieberwirth, C.; Seitz, H. Process and Installation for Manufacturing the Additive of Amorphous Crystalline and/or Semi-Crystalline Metal Components—Selective Amorphous Metal Extrusion (SAME). DE Patent 201410018080, 6 December 2014.
33. AIM3D GmbH. Edelstahl. 2017. Available online: <http://www.aim3d.de/Materialien/Edelstaehle/> (accessed on 7 July 2017).
34. Pollen AM Inc. Meet PAM: Pellet Additive Manufacturing. Available online: <https://www.pollen.am> (accessed on 22 August 2017).
35. Koslow, T. Pollen Introduces Pam: Their New Professional-Grade Multi-Material 3D Printer. Available online: <https://3dprint.com/140595/Pollen-Pam-Multi-Material/> (accessed on 22 August 2017).
36. Li, L.; Tirado, A.; Nlebedim, I.C.; Rios, O.; Post, B.; Kunc, V.; Lowden, R.R.; Lara-Curzio, E.; Fredette, R.; Ormerod, J.; et al. Big Area Additive Manufacturing of High Performance Bonded NdFeB Magnets. *Sci. Rep.* **2016**, *6*, 36212. [CrossRef]
37. Cincinnati Inc. BAAM: Fact Sheet. Available online: <https://wwwassets.e-ci.com/PDF/Products/baam-fact-sheet.pdf> (accessed on 7 June 2017).
38. Godec, D.; Cano, S.; Holzer, C.; Gonzalez-Gutierrez, J. Optimization of the 3D Printing Parameters for Tensile Properties of Specimens Produced by Fused Filament Fabrication of 17-4PH Stainless Steel. *Materials* **2020**, *13*, 774. [CrossRef] [PubMed]
39. Galati, M.; Minetola, P. Analysis of Density, Roughness, and Accuracy of the Atomic Diffusion Additive Manufacturing (ADAM) Process for Metal Parts. *Materials* **2019**, *12*, 4122. [CrossRef] [PubMed]
40. Bouaziz, M.A.; Djouda, J.M.; Kauffmann, J.; Hild, F. Microscale Mechanical Characterization of 17-4PH Stainless Steel Fabricated by Atomic Diffusion Additive Manufacturing (ADAM). *Procedia Struct. Integr.* **2020**, *28*, 1039–1046. [CrossRef]
41. Singh, G.; Missiaen, J.-M.; Bouvard, D.; Chaix, J.-M. Additive Manufacturing of 17–4 PH Steel Using Metal Injection Molding Feedstock: Analysis of 3D Extrusion Printing, Debinding and Sintering. *Addit. Manuf.* **2021**, *47*, 102287. [CrossRef]
42. Strano, M.; Rane, K.; Farid, M.A.; Mussi, V.; Zaragoza, V.; Monno, M. Extrusion-Based Additive Manufacturing of Forming and Molding Tools. *Int. J. Adv. Manuf. Technol.* **2021**. [CrossRef]
43. Kurose, T.; Abe, Y.; Santos, M.V.A.; Kanaya, Y.; Ishigami, A.; Tanaka, S.; Ito, H. Influence of the Layer Directions on the Properties of 316L Stainless Steel Parts Fabricated through Fused Deposition of Metals. *Materials* **2020**, *13*, 2493. [CrossRef]
44. Poszvek, G.; Stattler, G.; Markl, E.; Seemann, R.; Lackner, M. Fused Filament Fabrication of Metallic Components for Semi-Professional and Home Use. In Proceedings of the Digital Conversion on the Way to Industry 4.0, Online, Turkey, 24–26 September 2020; Durakbasa, N.M., Gençyilmaz, M.G., Eds.; Springer International Publishing: Cham, Switzerland, 2021; pp. 140–149.
45. Hassan, W.; Farid, M.A.; Tosi, A.; Rane, K.; Strano, M. The Effect of Printing Parameters on Sintered Properties of Extrusion-Based Additively Manufactured Stainless Steel 316L Parts. *Int. J. Adv. Manuf. Technol.* **2021**, *114*, 3057–3067. [CrossRef]
46. Sadaf, M. Additive Manufacturing of Metals Via Material Extrusion: Ph. D. Program in Design, Manufacturing, and Operation Engineering. Ph.D. Thesis, Università degli Studi di Roma Tor Vergata, Rome, Italy, 2022.
47. Heaney, D.F. *Powders for Metal Injection Molding (MIM)*, In *Handbook of Metal Injection Molding*; Heaney, D.F., Ed.; Woodhead Publishing: Cambridge, UK, 2012.

48. Engström, S. Metal Injection Molding: A Review of the MIM Process and Its Optimization. Master's Thesis, Arcada University of Applied Sciences, Helsinki, Finland, 2017.
49. Beran, T.; Mulholland, T.; Henning, F.; Rudolph, N.; Osswald, T.A. Nozzle Clogging Factors during Fused Filament Fabrication of Spherical Particle Filled Polymers. *Addit. Manuf.* **2018**, *23*, 206–214. [[CrossRef](#)]
50. Gonzlez-Gutierrez, J.; Beulke, G.; Emri, I. Powder Injection Molding of Metal and Ceramic Parts. In *Some Critical Issues for Injection Molding*; IntechOpen: London, UK, 2012; pp. 65–86.
51. Nötzel, D.; Eickhoff, R.; Hanemann, T. Fused Filament Fabrication of Small Ceramic Components. *Materials* **2018**, *11*, 1463. [[CrossRef](#)]
52. Kariz, M.; Sernek, M.; Obućina, M.; Kuzman, M.K. Effect of Wood Content in FDM Filament on Properties of 3D Printed Parts. *Mater. Today Commun.* **2018**, *14*, 135–140. [[CrossRef](#)]
53. Kukla, C.; Gonzalez-Gutierrez, J.; Duretek, I.; Schuschnigg, S.; Holzer, C.; Kukla, C.; Gonzalez-gutierrez, J.; Duretek, I. Effect of Particle Size on the Properties of Highly-Filled Polymers for Fused Filament Fabrication. In Proceedings of the American Institute of Physics, Provo, UT, USA, 16–21 July 2017; Volume 19, pp. 2–5.
54. Brostow, W.; Buchman, A.; Buchman, E.; Olea-mejia, O. Microhybrids of Metal Powder Incorporated in Polymeric Matrices: Friction, Mechanical Behavior, and Microstructure. *Pol. Eng. Sci.* **2008**, *48*, 1977–1981. [[CrossRef](#)]
55. Rang, Y.; Jaewoo, U.; Kwang, K.; Son, J. Effect of Particle Size, Dispersion, and Particle–Matrix Adhesion on W Reinforced Polymer Composites. *Res. Chem. Intermed.* **2014**, *40*, 2145–2153. [[CrossRef](#)]
56. Singh, P.; Balla, V.K.; Gokce, A.; Atre, S.V.; Kate, K.H. Additive Manufacturing of Ti-6Al-4V Alloy by Metal Fused Filament Fabrication (MF3): Producing Parts Comparable to That of Metal Injection Molding. *Prog. Addit. Manuf.* **2021**, *6*, 593–606. [[CrossRef](#)]
57. Contreras, J.M.; Jiménez-Morales, A.; Torralba, J.M. Experimental and Theoretical Methods for Optimal Solids Loading Calculation in MIM Feedstocks Fabricated from Powders with Different Particle Characteristics. *Powder Metall.* **2010**, *53*, 34–40. [[CrossRef](#)]
58. Sadaf, M.; Bragaglia, M.; Nanni, F. A Simple Route for Additive Manufacturing of 316L Stainless Steel via Fused Filament Fabrication. *J. Manuf. Process.* **2021**, *67*, 141–150. [[CrossRef](#)]
59. Damon, J.; Dietrich, S. Process Porosity and Mechanical Performance of Fused Filament Fabricated 316L Stainless Steel. *Rapid Prototyp. J.* **2019**, *7*, 1319–1327. [[CrossRef](#)]
60. Thompson, Y.; Gonzalez-Gutierrez, J.; Kukla, C.; Felfer, P. Fused Filament Fabrication, Debinding and Sintering as a Low Cost Additive Manufacturing Method of 316L Stainless Steel. *Addit. Manuf.* **2019**, *30*, 220–228. [[CrossRef](#)]
61. Gong, H.; Snelling, D.; Kardel, K.; Carrano, A. Comparison of Stainless Steel 316L Parts Made by FDM- and SLM-Based Additive Manufacturing Processes. *Solid Free. Fabr.* **2019**, *71*, 880–885. [[CrossRef](#)]
62. Ecker, J.V.; Dobrezberger, K.; Gonzalez-Gutierrez, J.; Spoerk, M.; Gierl-Mayer, C.; Danninger, H. Additive Manufacturing of Steel and Copper Using Fused Layer Modelling: Material and Process Development. *Powder Metall. Prog.* **2020**, *19*, 63–81. [[CrossRef](#)]
63. Tosto, C.; Tirillò, J.; Sarasini, F.; Cicala, G. Hybrid Metal/Polymer Filaments for Fused Filament Fabrication (FFF) to Print Metal Parts. *Appl. Sci.* **2021**, *11*, 1444. [[CrossRef](#)]
64. Gonzalez-Gutierrez, J.; Arbeiter, F.; Schlauf, T.; Kukla, C.; Holzer, C. Tensile Properties of Sintered 17-4PH Stainless Steel Fabricated by Material Extrusion Additive Manufacturing. *Mater. Lett.* **2019**, *248*, 165–168. [[CrossRef](#)]
65. Wu, G.; Langrana, N.A.; Sadanji, R.; Danforth, S. Solid Freeform Fabrication of Metal Components Using Fused Deposition of Metals. *Mater. Des.* **2002**, *23*, 97–105. [[CrossRef](#)]
66. Agarwala, M.K.; Van Weeren, R.; Bandyopadhyay, A.; Safari, A.; Danforth, S.C.; Priedeman, W.R. Filament Feed Materials for Fused Deposition Processing of Ceramics and Metals. *Solid Free. Fabr. Symp.* **1996**, *7*, 451–458.
67. Gonzalez-Gutierrez, J.; Godec, D.; Kukla, C.; Schlauf, T.; Burkhardt, C.; Holzer, C. Shaping, Debinding and Sintering of Steel Components Via Fused Filament Fabrication. In Proceedings of the 16th International Scientific Conference on Production Engineering—CIM2017, Zadar, Croatia, 8–10 June 2017; pp. 99–104.
68. Zhang, Y.; Roch, A. Fused Filament Fabrication and Sintering of 17-4PH Stainless Steel. *Manuf. Lett.* **2022**, *33*, 29–32. [[CrossRef](#)]
69. Giberti, H.; Strano, M.; Annoni, M. An Innovative Machine for Fused Deposition Modeling of Metals and Advanced Ceramics. *MATEC Web Conf.* **2016**, *43*, 03003. [[CrossRef](#)]
70. Taha, B.; Patil, S.; Dennis, B.H. Design and Manufacturing of Topology Optimized Heat Sinks Made of Copper Using 3D Printing. In Proceedings of the ASME 2021 16th International Manufacturing Science and Engineering Conference, Virtual, 21–25 June 2021; p. 8.
71. Moritzer, E.; Elsner, C.L. Investigation and Improvement of Processing Parameters of a Copper-Filled Polymer Filament in Fused Filament Fabrication as a Basis for the Fabrication of Low-Porosity Metal Parts. *Macromol. Symp.* **2022**, *404*, 2100390. [[CrossRef](#)]
72. Dehdari Ebrahimi, N.; Ju, Y.S. Thermal Conductivity of Sintered Copper Samples Prepared Using 3D Printing-Compatible Polymer Composite Filaments. *Addit. Manuf.* **2018**, *24*, 479–485. [[CrossRef](#)]
73. Ren, L.; Zhou, X.; Song, Z.; Zhao, C.; Liu, Q.; Xue, J.; Li, X. Process Parameter Optimization of Extrusion-Based 3D Metal Printing Utilizing PW-LDPE-SA Binder System. *Materials* **2017**, *10*, 305. [[CrossRef](#)] [[PubMed](#)]
74. Gonzalez-Gutierrez, J.; Cano, S.; Ecker, J.V.; Kitzmantel, M.; Arbeiter, F.; Kukla, C.; Holzer, C. Bending Properties of Lightweight Copper Specimens with Different Infill Patterns Produced by Material Extrusion Additive Manufacturing, Solvent Debinding and Sintering. *Appl. Sci.* **2021**, *11*, 7262. [[CrossRef](#)]

75. Sadaf, M.; Cano, S.; Gonzalez-Gutierrez, J.; Bragaglia, M.; Schuschnigg, S.; Kukla, C.; Holzer, C.; Vály, L.; Kitzmantel, M.; Nanni, F. Influence of Binder Composition and Material Extrusion (MEX) Parameters on the 3D Printing of Highly Filled Copper Feedstocks. *Polymers* **2022**, *14*, 4962. [CrossRef] [PubMed]
76. Sadaf, M. Thermoplastic-Based 3D Printable Highly Filled Filaments For Fused Filament Fabrication. In Proceedings of the 7th Young Polymer Scientists Conference and Short Course, Lodz, Poland, 27–28 September 2021.
77. Temple, S.G. Recent Developments in Properties and Protection of Copper for Electrical Uses. *Metall. Rev.* **1966**, *11*, 47–60. [CrossRef]
78. Perales-Rondon, J.V.; Rojas, D.; Gao, W.; Pumera, M. Copper 3D-Printed Electrodes for Ammonia Electrosynthesis via Nitrate Reduction. *ACS Sustain. Chem. Eng.* **2023**, *11*, 6923–6931. [CrossRef]
79. Redondo, E.; Pumera, M. Fully Metallic Copper 3D-Printed Electrodes via Sintering for Electrocatalytic Biosensing. *Appl. Mater. Today* **2021**, *25*, 101253. [CrossRef]
80. Singh, P.; Shaikh, Q.; Balla, V.K.; Atre, S.V.; Kate, K.H. Estimating Powder-Polymer Material Properties Used in Design for Metal Fused Filament Fabrication (DfMF3). *Jom* **2020**, *72*, 485–495. [CrossRef]
81. Thompson, Y.; Polzer, M.; Gonzalez-Gutierrez, J.; Kasian, O.; Heckl, J.P.; Dalbauer, V.; Kukla, C.; Felfer, P.J. Fused Filament Fabrication-based Additive Manufacturing of Commercially Pure Titanium. *Adv. Eng. Mater.* **2021**, *23*, 2100380. [CrossRef]
82. Singh, P.; Balla, V.K.; Atre, S.V.; German, R.M.; Kate, K.H. Factors Affecting Properties of Ti-6Al-4V Alloy Additive Manufactured by Metal Fused Filament Fabrication. *Powder Technol.* **2021**, *386*, 9–19. [CrossRef]
83. Zhang, Y.; Bai, S.; Riede, M.; Garratt, E.; Roch, A. A Comprehensive Study on Fused Filament Fabrication of Ti-6Al-4V Structures. *Addit. Manuf.* **2020**, *34*, 101256. [CrossRef]
84. Singh, P.; Balla, V.K.; Tofangchi, A.; Atre, S.V.; Kate, K.H. Printability Studies of Ti-6Al-4V by Metal Fused Filament Fabrication (MF3). *Int. J. Refract. Met. Hard Mater.* **2020**, *91*, 105249. [CrossRef]
85. Cruz, N.; Santos, L.; Vasco, J.; Barreiros, F.M. Binder System for Fused Deposition of Metals. In Proceedings of the International Powder Metallurgy Congress and Exhibition, Euro PM 2013, Gothenburg, Sweden, 23–25 January 2013.
86. Kukla, C.; Gonzalez-Gutierrez, J.; Burkhardt, C.; Weber, O.; Holzer, C. The Production of Magnets by FFF-Fused Filament Fabrication. In Proceedings of the Euro PM 2017: International Powder Metallurgy Congress and Exhibition, Milan, Italy, 1–5 October 2017.
87. Bek, M.; Gonzalez-Gutierrez, J.; Kukla, C.; Črešnar, K.P.; Maroh, B.; Perše, L.S. Rheological Behaviour of Highly Filled Materials for Injection Moulding and Additive Manufacturing: Effect of Particle Material and Loading. *Appl. Sci.* **2020**, *10*, 7993. [CrossRef]
88. Gonzalez-Gutierrez, J.; Duretek, I.; Holzer, C.; Arbeiter, F.; Kukla, C. Filler Content and Properties of Highly Filled Filaments for Fused Filament Fabrication of Magnets. In Proceedings of the Annual Technical Conference—ANTEC, Conference Proceedings, Anaheim, CA, USA, 8–10 May 2017; pp. 55–58.
89. Markforged Metal X-Datasheet. Available online: <https://markforged.com/3d-printers/metal-x> (accessed on 14 November 2022).
90. Md Ani, S.; Muchtar, A.; Muhamad, N.; Ghani, J.A. Binder Removal via a Two-Stage Debinding Process for Ceramic Injection Molding Parts. *Ceram. Int.* **2014**, *40*, 2819–2824. [CrossRef]
91. Tseng, W.J.; Hsu, C.-K. Cracking Defect and Porosity Evolution during Thermal Debinding in Ceramic Injection Moldings. *Ceram. Int.* **1999**, *25*, 461–466. [CrossRef]
92. Suwanpreecha, C.; Manonukul, A. A Review on Material Extrusion Additive Manufacturing of Metal and How It Compares with Metal Injection Moulding. *Metals* **2022**, *12*, 429. [CrossRef]
93. Cano, S.; Gonzalez-Gutierrez, J.; Sapkota, J.; Spoerk, M.; Arbeiter, F.; Schuschnigg, S.; Holzer, C.; Kukla, C. Additive Manufacturing of Zirconia Parts by Fused Filament Fabrication and Solvent Debinding: Selection of Binder Formulation. *Addit. Manuf.* **2019**, *26*, 117–128. [CrossRef]
94. Lengauer, W.; Duretek, I.; Fürst, M.; Schwarz, V.; Gonzalez-Gutierrez, J.; Schuschnigg, S.; Kukla, C.; Kitzmantel, M.; Neubauer, E.; Lieberwirth, C.; et al. Fabrication and Properties of Extrusion-Based 3D-Printed Hardmetal and Cermet Components. *Int. J. Refract. Met. Hard Mater.* **2019**, *82*, 141–149. [CrossRef]
95. Gorjan, L.; Galusca, C.; Sami, M.; Sebastian, T.; Clemens, F. Effect of Stearic Acid on Rheological Properties and Printability of Ethylene Vinyl Acetate Based Feedstocks for Fused Filament Fabrication of Alumina. *Addit. Manuf.* **2020**, *36*, 101391. [CrossRef]
96. Gonzalez-Gutierrez, J.; Guráň, R.; Spoerk, M.; Holzer, C.; Godec, D.; Kukla, C. 3D Printing Conditions Determination for Feedstock Used in Fused Filament Fabrication (FFF) of 17-4PH Stainless Steel Parts. *Metalurgija* **2018**, *57*, 117–120.
97. Kukla, C.; Gonzalez-Gutierrez, J.; Cano, S.; Hampel, S. Fused Filament Fabrication (FFF) of PIM Feedstocks. In Proceedings of the VI Congreso Nacional de Pulvimetallurgia y I Congreso Iberoamericano de Pulvimetallurgia, Ciudad Real, Spain, 15 February 2017; pp. 7–9.
98. Abel, J.; Scheithauer, U.; Janics, T.; Hampel, S.; Cano, S.; Müller-Köhn, A.; Günther, A.; Kukla, C.; Moritz, T. Fused Filament Fabrication (FFF) of Metal-Ceramic Components. *J. Vis. Exp.* **2019**, *2019*, e57693. [CrossRef]
99. Bandyopadhyay, A.; Das, K.; Marusich, J.; Onagoruwa, S. Application of Fused Deposition in Controlled Microstructure Metal-Ceramic Composites. *Rapid Prototyp. J.* **2006**, *12*, 121–128. [CrossRef]
100. Gloeckle, C.; Konkol, T.; Jacobs, O.; Limberg, W.; Ebel, T.; Handge, U.A. Processing of Highly Filled Polymer-Metal Feedstocks for Fused Filament Fabrication and the Production of Metallic Implants. *Materials* **2020**, *13*, 4413. [CrossRef] [PubMed]
101. Clemens, F. Thermoplastic Extrusion for Ceramic Bodies. In *Extrusion in Ceramics*; Springer: Berlin/Heidelberg, Germany, 2009; pp. 295–311, ISBN 9783540271024.

102. Kukla, C.; Gonzalez-Gutierrez, J.; Felfer, P.; Holzer, C. Material Extrusion with Filaments for the Production of Metal Parts and Feedstock Therefore. In Proceedings of the Metal Additive Manufacturing, Vienna, Austria, 21–23 November 2018; Volume 4, pp. 1–9.
103. Venkataraman, N.; Rangarajan, S.; Mathewson, M.J.; Safari, A.; Danforth, S.C.; Yardimci, A. Mechanical and Rheological Properties of Feedstock Material for Fused Deposition of Ceramics and Metals (FDC and FDMet) and Their Relationship to Process Performance. In Proceedings of the International Solid Freeform Fabrication Symposium, Austin, TX, USA, 9–11 August 1999; pp. 351–359.
104. Galantucci, L.; Pellegrini, A.; Guerra, M.; Lavecchia, F. 3D Printing of Parts Using Metal Extrusion: An Overview of Shaping, Debinding and Sintering Technology. *Adv. Technol. Mater.* **2022**, *47*, 25–32. [CrossRef]
105. Vurpillat, J. 3D Demonstrators Designed for Bigger, Lighter Auto and Aerospace Parts. Available online: <http://blog.stratasys.com/2016/08/24/infinite-build-robotic-composite-3d-demonstrator/> (accessed on 25 August 2016).
106. Kochan, A. Feature Rapid Growth for Rapid Prototyping. *Assem. Autom.* **1997**, *17*, 215–217. [CrossRef]
107. Riecker, S.; Clouse, J.; Studnitzky, T.; Andersen, O.; Kieback, B. Fused Deposition Modeling—Opportunities for Cheap Metal AM. In Proceedings of the World PM2016 Congress Exhibition, Hamburg, Germany, 9–13 October 2016. [CrossRef]
108. Burkhardt, C. Fused Filament Fabrication (FFF) of 316L Green Parts for the MIM Process. In Proceedings of the World PM2016—M—Deposition Technologies, Hamburg, Germany, 9–13 October 2016.
109. Rinaldi, M.; Ghidini, T.; Cecchini, F.; Branda, A.; Nanni, F. Additive Layer Manufacturing of Poly (Ether Ether Ketone) via FDM. *Compos. Part B Eng.* **2018**, *145*, 162–172. [CrossRef]
110. Popescu, D.; Zapciu, A.; Amza, C.; Baciu, F.; Marinescu, R. FDM Process Parameters in Fluence over the Mechanical Properties of Polymer Specimens: A Review. *Polym. Test.* **2018**, *69*, 157–166. [CrossRef]
111. Spoerk, M.; Gonzalez-Gutierrez, J.; Sapkota, J.; Schuschnigg, S.; Holzer, C. Effect of the Printing Bed Temperature on the Adhesion of Parts Produced by Fused Filament Fabrication. *Plast. Rubber Compos.* **2018**, *47*, 17–24. [CrossRef]
112. Singh, G.; Missiaen, J.M.; Bouvard, D.; Chaix, J.M. Copper Extrusion 3D Printing Using Metal Injection Moulding Feedstock: Analysis of Process Parameters for Green Density and Surface Roughness Optimization. *Addit. Manuf.* **2021**, *38*, 101778. [CrossRef]
113. Gonzalez-Gutierrez, J.; Cano Cano, S.; Schuschnigg, S.; Holzer, C.; Kukla, C. Highly-Filled Polymers for Fused Filament Fabrication. In Proceedings of the Leobener Kunststoff-Kolloquium, Leoben, Austria, 19–20 April 2018; pp. 93–104.
114. Heaney, D.F. *Handbook of Metal Injection Molding*; Woodhead Publishing: Sawston, UK, 2018; ISBN 0081021534.
115. Zaky, M.T. Effect of Solvent Debinding Variables on the Shape Maintenance of Green Molded Bodies. *J. Mater. Sci.* **2004**, *39*, 3397–3402. [CrossRef]
116. ASM. *International Handbook Committee Powder Metal Technologies and Applications*; ASM International: Detroit, MI, USA, 2010; Volume 7, pp. 1–16.
117. George, E.; Robert, D. Deformation Processing of Sintered Powder Materials. In *Powder Metallurgy Processing: New Techniques and Analyses*; Academic Press: Cambridge, MA, USA, 2012; pp. 99–138. ISBN 0124284507.
118. Mirzababaei, S.; Pasebani, S. A Review on Binder Jet Additive Manufacturing of 316L Stainless Steel. *J. Manuf. Mater. Process.* **2019**, *3*, 82. [CrossRef]
119. Kong, L.B.; Huang, Y.; Que, W.; Zhang, T.; Li, S.; Zhang, J.; Dong, Z.; Tang, D. *Sintering and Densification (I)—Conventional Sintering Technologies*; Springer: Berlin/Heidelberg, Germany, 2015; ISBN 9783319189567.
120. Kang, S.-J.L. Basis of Sintering Science. In *Sintering Densification, Grain Growth and Microstructure*; Elsevier: Amsterdam, The Netherlands, 2005; pp. 261–265.
121. Bhaduri, S. Review of: “POWDER INJECTION MOLDING” by R.M. German Metal Powder Industries Federation American Powder Metallurgy Institute 105, College Road East, Princeton, New Jersey 08540 544 Pages, \$75, Hardbound, 1990. *Mater. Manuf. Process.* **1992**, *7*, 139–140. [CrossRef]
122. Kong, X. Powder Feedstocks for Micro-Injection Molding. *Microsyst. Technol.* **2013**, *8*, 129–132. [CrossRef]
123. Várez, A.; Levenfeld, B.; Torralba, J.M.; Matula, G.; Dobrzanski, L.A. Sintering in Different Atmospheres of T15 and M2 High Speed Steels Produced by a Modified Metal Injection Moulding Process. *Mater. Sci. Eng. A* **2004**, *366*, 318–324. [CrossRef]
124. Pease, L.F.; West, W.G. Sintering. In *Fundamentals of Powder Metallurgy*; Metal Powder Industry: Princeton, NJ, USA, 2002; pp. 220–245. ISBN 1878954865.
125. Lous, G.M.; Cornejo, I.A.; McNulty, T.F.; Safari, A.; Danforth, S.C. Fabrication of Curved Ceramic/Polymer Composite Transducer for Ultrasonic Imaging Applications by Fused Deposition of Ceramics. In Proceedings of the IEEE International Symposium on Applications of Ferroelectronics (ISAF), Montreux, Switzerland, 24–27 August 1998; pp. 239–242. [CrossRef]
126. Agarwala, M.K. Structural Quality of Parts Processed by Fused Deposition. *Rapid Prototyp. J.* **1996**, *2*, 4–19. [CrossRef]
127. Huang, M.-S.; Hsu, H.-C. Influence of Injection Moulding and Sintering Parameters on Properties of 316L MIM Compact. *Powder Metall.* **2011**, *54*, 299–307. [CrossRef]
128. Krug, S.; Evans, J.R.G.; Ter Maat, J.H.H. Differential Sintering in Ceramic Injection Moulding: Particle Orientation Effects. *J. Eur. Ceram. Soc.* **2002**, *22*, 173–181. [CrossRef]
129. Guazzato, M.; Proos, K.; Quach, L.; Swain, M.V. Strength, Reliability and Mode of Fracture of Bilayered Porcelain/Zirconia (Y-TZP) Dental Ceramics. *Biomaterials* **2004**, *25*, 5045–5052. [CrossRef] [PubMed]

130. Desktop Metal Launches the Studio System 2 3d Printer Technical Specifications and Pricing-183766. Available online: <https://3dprintingindustry.com/news/desktop-metal-launches-the-studio-system-2-3d-printer-technical-specifications-and-pricing-183766/> (accessed on 14 November 2022).
131. Williams, B. Ceramic Injection Moulding and Ceramic Additive Manufacturing Side by Side: Opportunities and Challenges. *Powder Inject. Mould. Int.* **2018**, *12*, 77–84.
132. Safka, J.; Ackermann, M.; Machacek, J.; Seidl, M.; Vele, F.; Truxova, V. Fabrication Rrocess and Basic Material Properties of the Basf Ultrafuse 316Lx Material. *MM Sci. J.* **2020**, *2020*, 4216–4222. [CrossRef]
133. Zocca, A.; Colombo, P.; Gomes, C.M.; Günster, J. Additive Manufacturing of Ceramics: Issues, Potentialities, and Opportunities. *J. Am. Ceram. Soc.* **2015**, *98*, 1983–2001. [CrossRef]
134. Carminati, M.; Quarto, M.; D'Urso, G.; Giardini, C.; Borriello, C. A Comprehensive Analysis of AISI 316L Samples Printed via FDM: Structural and Mechanical Characterization. *Key Eng. Mater.* **2022**, *926*, 46–55. [CrossRef]
135. Carminati, M.; Quarto, M.; D'Urso, G.; Giardini, C.; Maccarini, G. Mechanical Characterization of AISI 316L Samples Printed Using Material Extrusion. *Appl. Sci.* **2022**, *12*, 1433. [CrossRef]
136. Gong, H.; Crater, C.; Ordonez, A.; Ward, C.; Waller, M.; Ginn, C. Material Properties and Shrinkage of 3D Printing Parts Using Ultrafuse Stainless Steel 316LX Filament. *Funct. Mater. Des. Dev.* **2018**, *249*, 1001. [CrossRef]
137. Pellegrini, A.; Palmieri, M.; Guerra, M. Evaluation of Anisotropic Mechanical Behaviour of 316L Parts Realized by Metal Fused Filament Fabrication Using Digital Image Correlation. *Int. J. Adv. Manuf. Technol.* **2022**, *120*, 7951–7965. [CrossRef]
138. Spiller, S.; Kolstad, S.O.; Razavi, N. Fabrication and Characterization of 316L Stainless Steel Components Printed with Material Extrusion Additive Manufacturing. *Procedia Struct. Integr.* **2022**, *42*, 1239–1248. [CrossRef]
139. Ji, S.; Gu, Q.; Xia, B. Porosity Dependence of Mechanical Properties of Solid Materials. *J. Mater. Sci.* **2006**, *41*, 1757–1768. [CrossRef]
140. Kheiri, S.; Mirzadeh, H.; Naghizadeh, M. Tailoring the Microstructure and Mechanical Properties of AISI 316L Austenitic Stainless Steel via Cold Rolling and Reversion Annealing. *Mater. Sci. Eng. A* **2019**, *759*, 90–96. [CrossRef]
141. Zhang, Y.; Feng, E.; Mo, W.; Lv, Y.; Ma, R.; Ye, S.; Wang, X.; Yu, P. On the Microstructures and Fatigue Behaviors of 316L Stainless Steel Metal Injection Molded with Gas-and Water-Atomized Powders. *Metals* **2018**, *8*, 893. [CrossRef]
142. Heaney, D.F.; Mueller, T.W.; Davies, P.A. Mechanical Properties of Metal Injection Moulded 316L Stainless Steel Using Both Prealloy and Master Alloy Techniques. *Powder Metall.* **2004**, *47*, 367–373. [CrossRef]
143. Saboori, A.; Aversa, A.; Marchese, G.; Biamino, S.; Lombardi, M.; Fino, P. Microstructure and Mechanical Properties of AISI 316L Produced by Directed Energy Deposition-Based Additive Manufacturing: A Review. *Appl. Sci.* **2020**, *10*, 3310. [CrossRef]
144. Guo, P.; Zou, B.; Huang, C.; Gao, H. Study on Microstructure, Mechanical Properties and Machinability of Efficiently Additive Manufactured AISI 316L Stainless Steel by High-Power Direct Laser Deposition. *J. Mater. Process. Technol.* **2017**, *240*, 12–22. [CrossRef]
145. Röttger, A.; Boes, J.; Theisen, W.; Thiele, M.; Esen, C.; Edelmann, A.; Hellmann, R. Microstructure and Mechanical Properties of 316L Austenitic Stainless Steel Processed by Different SLM Devices. *Int. J. Adv. Manuf. Technol.* **2020**, *108*, 769–783. [CrossRef]
146. Chniouel, A.; Giroux, P.F.; Lomello, F.; Aubry, P.; Vasquez, É.; Hercher, O.; Maskrot, H. Influence of Substrate Temperature on Microstructural and Mechanical Properties of 316L Stainless Steel Consolidated by Laser Powder Bed Fusion. *Int. J. Adv. Manuf. Technol.* **2020**, *111*, 3489–3503. [CrossRef]
147. Lavery, N.P.; Cherry, J.; Mehmood, S.; Davies, H.; Girling, B.; Sackett, E.; Brown, S.G.R.; Sienz, J. Effects of Hot Isostatic Pressing on the Elastic Modulus and Tensile Properties of 316L Parts Made by Powder Bed Laser Fusion. *Mater. Sci. Eng. A* **2017**, *693*, 186–213. [CrossRef]
148. Thomas-Vielma, P.; Cervera, A.; Levenfeld, B. Production of Alumina Parts by Powder Injection Molding with a Binder System Based on High Density Polyethylene. *J. Eur. Ceram. Soc.* **2008**, *28*, 763–771. [CrossRef]
149. Choi, J.P.; Lee, G.Y.; Song, J.-I.; Lee, W.S.; Lee, J.S. Sintering Behavior of 316L Stainless Steel Micro-Nanopowder Compact Fabricated by Powder Injection Molding. *Powder Technol.* **2015**, *279*, 196–202. [CrossRef]
150. Busby, J.T.; Maziasz, P.J.; Rowcliffe, A.F.; Santella, M.; Sokolov, M. Development of High Performance Cast Stainless Steels for ITER Shield Module Applications. *J. Nucl. Mater.* **2011**, *417*, 866–869. [CrossRef]

**Disclaimer/Publisher's Note:** The statements, opinions and data contained in all publications are solely those of the individual author(s) and contributor(s) and not of MDPI and/or the editor(s). MDPI and/or the editor(s) disclaim responsibility for any injury to people or property resulting from any ideas, methods, instructions or products referred to in the content.